In vitro reconstitution of T cell receptor–mediated segregation of the CD45 phosphatase

Catherine B. Carbone[1], Nadja Kern[1], Ricardo A. Fernandes[2], Enfu Hui[1], Xiaolei Su[1], K. Christopher Garcia[2], and Ronald D. Vale[1]

[1]Dept. of Cellular and Molecular Pharmacology and the Howard Hughes Medical Institute, University of California San Francisco
[2]Dept. of Molecular and Cellular Physiology and Structural Biology and the Howard Hughes Medical Institute, Stanford University Medical School

Address correspondence to: ron.vale@ucsf.edu

ABSTRACT

Binding of the T cell receptor (TCR) to peptide-major histocompatibility complex (pMHC) initiates signaling leading to T cell activation. Signaling is proposed to be triggered by the segregation of the transmembrane phosphatase CD45 from TCR-pMHC, caused by a difference in sizes of their extracellular domains. Here, we have reconstituted the segregation of CD45 from TCR-pMHC using purified proteins on model membranes. Similar to the sensitivity of T cell signaling, TCR-pMHC interactions with Kds of ≤15 μM were needed to exclude CD45; the larger of two developmentally-regulated isoforms of CD45 was excluded more rapidly and efficiently. We further show that two receptor-ligand pairs, TCR-pMHC and the inhibitory co-receptor PD-1 with its ligand PD-L1, segregate from one another and together create zones of CD45 exclusion. These results demonstrate that the binding energy of TCR-pMHC at membrane-membrane interfaces is sufficient to create spatial partitioning of the TCR relative to CD45.

INTRODUCTION

Ligation of the TCR to agonist pMHC triggers a signaling cascade within the T cell leading to reorganization of the cytoskeleton and organelles, transcriptional changes, and cell proliferation. The first step in the cascade is TCR phosphorylation by the Src family tyrosine kinase Lck [Brownlie and Zamoyska, 2013]. One model, called "kinetic segregation" [Davis and van der Merwe, 2006], for how this initiating phosphorylation is triggered proposes that the close membrane contact created by TCR-pMHC binding results in exclusion of the inhibitory transmembrane phosphatase CD45 and therefore unopposed phosphorylation of the TCR by Lck. The basis of this exclusion is thought to be steric, since the large CD45 extracellular domain (CD45 R_0 isoform, 25nm; CD45 R_{ABC} isoform, 40nm, **supplementary table**) [Woollett, et al., 1985; McCall, et al., 1992; Chang, et al. 2016] may not be able to penetrate the narrow inter-membrane spacing generated by TCR-pMHC complex (13 nm, **supplementary table**) [Birnbaum, et al 2014]. CD45 exclusion from TCR-pMHC is observed in T cells [Varma, et al., 2006], and cellular reconstitutions have demonstrated that this size-dependent partitioning is necessary and sufficient for receptor phosphorylation [James and Vale, 2012; Cordoba, et al., 2013]. However, it is unclear whether the physical properties of CD45 and TCR-pMHC at the membrane-membrane interface alone are sufficient to explain the observed segregation behavior or whether other cellular factors (e.g. actin cytoskeletal or lipid ordering) are also required. Here, we have recapitulated TCR-pMHC mediated partitioning of CD45 on model membranes and show that affinity, size and inter-membrane spacing regulate the efficiency of partitioning.

RESULTS AND DISCUSSION

To mimic a T cell, we used a giant unilamellar vesicle (GUV) containing a nickel-chelating lipid to which a purified His-tagged, fluorescently-labeled receptor and CD45 could be added (**Fig. 1a**). To mimic the APC, we used a supported lipid bilayer (SLB) containing nickel-chelating lipids to which a His-tagged protein ligand also could be bound. As an initial test of this system, we used an artificial receptor (FKBP) and ligand (FRB) that could be induced to form a tight binding interaction (100 fM) upon addition of rapamycin [Banaszynski, et al., 2006]. In order to maintain the GUV and SLB in proximity prior to rapamycin addition, the two membranes were passively tethered to one another using two 100-mer single-stranded DNA molecules with a 20 bp region of complementarity [Taylor et al., 2016, Chi et al., 2013] (**supplementary table**). The

elongated extracellular domain of the CD45 R_0 isoform (25 nm) [Woollett, et al., 1985; McCall, et al., 1992; Chang, et al. 2016] or the smaller SNAP protein (5 nm, **supplementary table**) [Gautier, et al. 2008] were used as test proteins for partitioning. Upon rapamycin addition, FKBP and FRB concentrated first in small micron-scale clusters at the GUV-SLB interface, which then grew in size over the interface; simultaneously, fluorescently-labeled CD45 R_0 partitioned away from regions of the GUV that became enriched in receptor-ligand (**Fig 1b and Video 1**). In contrast, the SNAP protein remained evenly distributed throughout the interface after rapamycin addition (**Fig 1c-d**). The size of FKBP-FRB clusters could be varied by changing the receptor concentration on the GUV membrane; however, the degree of CD45 R_0 exclusion from clusters was similar over the range tested (**Fig 1e-f**). These results confirm earlier work that DNA-DNA [Chung, et al., 2013] or protein-protein [Schmid, et al., 2016] interactions can induce a size-dependent spatial reorganization of molecules at a GUV-SLB or GUV-GUV interface. In addition, this rapamycin-inducible system enables the observation of protein segregation at a GUV-SLB interface in real-time.

The kinetic segregation model predicts that CD45 is excluded from receptor-ligand complexes based upon a difference in the spacing between the GUV and SLB in the receptor- versus CD45-enriched regions [Davis and van der Merwe, 2006]. To reconstruct the topology of the GUV membrane across the interface with nanometer accuracy in the vertical axis, we used scanning angle interference microscopy (SAIM), a technique that calculates the distance of fluorophores from a silicon oxide wafer by collecting sequential images at multiple illumination angles (**Fig. 3a**) [Carbone, et al., 2016]. The SAIM reconstructions revealed membrane deformations at regions of CD45 localization (**Fig 3b-d**). The calculated difference in membrane spacing between the FRB-FKBP- and CD45 R_0 - enriched regions was 18 ± 11 nm, suggesting a size of ~24 nm for the CD45 R_0 extracellular domain, assuming that FRB-FKBP creates an intermembrane space of 6 nm (**supplementary table**)[Liang, et al., 1999]. Conversely, for GUV-SLB interfaces with FRB-FKBP and SNAP, SAIM reconstructions revealed no changes in membrane spacing across the GUV-SLB interface (**Fig. 3—figure supplement 1**).

Next, we sought to establish a GUV-SLB interface using the native T cell receptor-ligand pair, TCR-pMHC. For the TCR, we co-expressed the extracellular domains of the 2B4 α and β chains extended with leucine zippers to stabilize their dimerization [Birnbaum et al., 2014]; both chains were tagged with His_{10} for conjugation to the GUV membrane and the β chain contained a ybbR peptide for fluorescent labeling. For the ligand, we used the I-Ek MHC, His_{10}-tagged, and loaded

with a high affinity (2.5 μM Kd) peptide (**Fig 2a**). In addition to testing the CD45 R_0 isoform for segregation, we also compared the extracellular domain of the CD45 R_{ABC} isoform, which is preferentially expressed early in T cell development [Hermiston, et al., 2003], and is about 15 nm larger in size than the shorter and later expressed R_0 isoform (**Fig 2b, supplementary table**) [Woollett, et al., 1985; McCall et al., 1992]. Upon GUV contact with the SLB, the 2B4 TCR bound the I-Ek MHC, and concentrated at the interface where it formed micron-scale clusters that excluded both isoforms of CD45 but not the control SNAP domain (**Fig 2c—figure supplement 1**). Interestingly, the degree of TCR-pMHC mediated exclusion of the smaller CD45 R_0 isoform (9 ± 5%) was lower than the larger CD45 R_{ABC} isoform (32 ± 5%) at steady state (45 min)(**Fig 2c**). To investigate potential temporal differences in exclusion between the two CD45 isoforms, we employed the chemically-inducible FRB-FKBP partitioning system. With both isoforms present on the same GUV, the larger CD45 R_{ABC} isoform segregated from newly forming FKBP clusters three-fold faster than the R_0 isoform (**Fig 2—figure supplement 1**). In contrast to the TCR-pMHC system, we found no difference in the final extent of exclusion between the two CD45 isoforms with the higher affinity FRB-FKBP system (**Fig 2—figure supplement 2**).

In vivo, TCR encounters MHCs loaded with a myriad of different peptides; although not absolute, TCR-pMHC affinities of <50 uM are usually required to trigger a signaling response [Gascoigne, et al., 2001]. To examine the effect of TCR-pMHC affinity on CD45 R_{ABC} exclusion, we loaded I-Ek MHC with a series of well-characterized peptides with resultant affinities of 2.5 μM, 7.7 μM, 15 μM, 50 μM and null for the 2B4 TCR [Birnbaum, et al., 2014]. At steady state, we observed similar CD45 R_{ABC} exclusion for pMHCs with affinities to the TCR of 15 μM and lower; however, the pMHC with a Kd of 50 μM and I-Ek loaded with null peptides did not concentrate TCR at the GUV-SLB interface and did not change the distribution of CD45 R_{ABC} (**Fig 2d**). Thus CD45 R_{ABC} exclusion was observed over the same range of affinities that are associated with peptide agonists.

T cell signaling involves many receptor-ligand pairs interacting across the two membranes in addition to the TCR-pMHC [Chen and Flies, 2013]. To create a simple mimic of this complex system, along with the TCR-pMHC, we included a second receptor-ligand pair—the inhibitory co-receptor PD-1 and its ligand PD-L1. The PD-1-PD-L1 complex shares a similar dimension to the TCR-pMHC complex (9 nm, **supplementary table**) [Lin, et al., 2008] and has a slightly higher affinity (0.77 μM) [Butte, et al., 2013]. Like the FRB-FKBP and TCR-pMHC systems, PD-

1-PD-L1 alone formed micron-sized clusters that excluded CD45 R_{ABC} (CD45 exclusion: 19 ± 7%, **Fig. 4a**). Interestingly, in the dual receptor-ligand system, PD-1 segregated from TCR enriched regions (33 ± 8% exclusion) and CD45 R_{ABC} was partitioned away from the combined ligated TCR-PD-1 footprint (**Fig. 4a,** bottom, **4b-c**).

In summary, we have established an *in vitro* membrane system that recapitulates TCR-pMHC mediated CD45 exclusion. We observed that size, affinity, and inter-membrane spacing control the efficiency of protein partitioning. These results demonstrate that the biophysical constraints at a membrane-membrane contact are sufficient for CD45 segregation from bound TCR-pMHC complexes. While these findings do not exclude the possibility that lipid-mediated and intracellular mechanisms may enhance CD45 partitioning *in vivo* [Miceli, et al., 2001; Su, et al, 2016], our results support the kinetic segregation model [Davis and van der Merwe, 2006] in which receptor-ligand binding and membrane bending alone can give rise to spatial organization.

Our results also demonstrate that the large extracellular domains of CD45 R_{ABC} and CD45 R_0 are differentially sensitive to the partitioning forces produced by ligand-receptor binding interactions at a membrane-membrane interface. This finding is consistent with results showing that T cells expressing larger CD45 isoforms signal more efficiently [Chui, et al., 1994], although others have contested this conclusion [Czyzyk, et al., 2000]. Though the signaling consequences of differential CD45 segregation on immune activation remain to be clarified, our results establish a difference between two highly conserved CD45 isoforms [Okumura, et al., 1996] with regard to their degree of spatial segregation in response to TCR-pMHC interactions.

Finally, our finding that PD1-PD-L1 segregates from TCR-pMHC *in vitro* is supported by the result that PD-1-PD-L1 partially segregates from TCR-pMHC in CD8+ T cells [Hui, et al., 2016]. The basis of this inhomogeneous distribution is not known, but could involve the 4 nm difference in inter-membrane sizes (**Fig. 4d, supplementary table**), different kinetics of interaction, or different affinities between the receptor-ligand complexes. Conceivably, the principles of kinetic segregation also may provide a mechanism for regulating co-receptors by partitioning their biochemical activities in different regions of the membrane.

MATERIALS AND METHODS

Materials

Synthetic 1,2-dioleoyl-sn-glycero-3-phosphocholine (POPC; Avanti, 850457), 1,2-dioleoyl-sn-glycero-3-[(N-(5-amino-1-carboxypentyl)iminodiacetic acid)succinyl] (nickel salt, DGS-NTA-Ni; Avanti, 790404) and 1,2-dioleoyl-sn-glycero-3-phosphoethanolamine-N [methoxy(polyethylene glycol)-5000] (ammonium salt, PEG5000-PE; Avanti, 880220) were acquired from Avanti Polar Lipids, Alabama, USA. 1,2-dioleoyl-sn-glycero-3-phosphoethanolamine-Atto390 (DOPE-390; AttoTec, AD390-161) was acquired from Atto-Tec, Germany.

Recombinant protein expression, purification, and labeling

N-terminally His_{10}- and SNAP- tagged FRB and FKBP were subcloned into a pET28a vector and were bacterially expressed in BL21(DE3) strain of *Escherichia coli*. The cells were lysed in an Avestin Emulsiflex system. C-terminally His_{10}- and SNAP- tagged extracellular domains of human CD45 R_0, human CD45 R_{ABC}, and human PD-L1 were subcloned into a pFastBac vector and were expressed in SF9 cells. All proteins were purified by using a HisTrap excel column following the product recommendations. Recombinant C terminally His_{10} tagged mouse PD-1 extracellular domain was purchased from Sino Biological.

2B4 TCR V_mC_h chimeras containing an engineered C domain disulfide were cloned into the pAcGP67a insect expression vector (BD Biosciences, 554756) encoding either a C-terminal acidic GCN4-zipper-Biotin acceptor peptide (BAP)-6xHis tag (for α chain) or a C-terminal basic GCN4 zipper-6xHis tag (for β chain) [Wilson, et al., 1999]. Each chain also encoded a 3C protease site between the C-terminus of the TCR ectodomains and the GCN4 zippers to allow for cleavage of zippers. I-Ek MHC was cloned into pAcGP67A with acidic/basic zippers as described for TCRs. I-Ek α and 2B4 α chain also encoded ybbr-tag sequence for direct protein labelling. The I-Ekβ construct was modified with an N-terminal extension containing either the 2A peptide via a Gly-Ser linker or CLIP peptide via a Gly-Ser linker containing a thrombin cleavage site. Proteins were transiently expressed in High Five insect cells (BTI-TN-5B1-4) and purified using His-tag/Nickel according to published protocols [Birnbaum, et al., 2014].

For fluorescent labeling of SNAP-tagged proteins, 10 μM protein was incubated with 20 μM benzylguanine functionalized dye (New England Biolabs) in HBS buffer (50 mM HEPES, 150 mM NaCl, 1 mM TCEP, pH 7.4) for 1 h at room temperature or overnight on ice. For PD-L1 and TCR 10 μM protein was incubated with 30 μM tetramethylrhodamine-5-maleimide in HBS buffer for 1 h at room temperature. Excess dyes were removed using Zeba Spin Desalting Columns (ThermoFisher, 89882).

Preparation of SNAP-DNA tethers

Oligonucleotides were ordered from IDT with a 3'/5' terminal amine and labeled with BG-GLA-NHS as previously described [Farlow, et al., 2013]. The adhesion strands used in this study consisted of a 3' 20mer region (5'- ACTGACTGACTGACTGACTG-3') with a 5' 80mer poly-dT and the complementary sequence (5'- CAGTCAGTCAGTCAGTCAGT-3') also with a 5' 80mer poly-dT. Conjugation to benzyl-guanine was performed as described [Farlow, et al., 2013]. His_{10}-tagged SNAP was labeled at a concentration of 5 μM with a 3-fold excess of BG-DNA in HBS (50 mM HEPES, 150 mM NaCl and 1 mM TCEP, pH 7.4).

Electroformation of giant unilamellar vesicles

Lipids were mixed with a molar composition of 94.9% POPC, 5% DGS-NTA, 0.1% DOPE-390 in chloroform (Electron Microscopy Sciences, 12550) and dried under vacuum for 1 h to overnight. Electroformation was performed in 370 mM sucrose according to published protocols [Schmid, et al., 2015]. GUVs were stored at room temperature and imaged within one week.

Preparation of supported lipid bilayers

Small unilamellar vesicles (SUVs) were prepared from a mixture of 95.5% POPC, 2% DGS-NGA-Ni, and 0.5% PEG5000-PE. The lipid mixture in chloroform was evaporated under argon and further dried under vacuum. The mixture was then rehydrated with phosphate buffered saline pH 7.4 and cycled between -80°C and 37°C 20 times, and then centrifuged for 45 min at 35,000 RCF. SUVs made by this method were stored at 4°C and used within two weeks of formation. Supported lipid bilayers were formed in freshly plasma cleaned custom PDMS chambers on RCA cleaned glass coverslips. 100 μl of SUV solution containing 0.5 to 1 mg/ml lipid was added to the coverslips and incubated for 30 min. Unadsorbed vesicles were removed

and bilayers were blocked by washing three times with reaction buffer (50 mM HEPES, 150 mM NaCl, 1 mM TCEP, 1 mg/mL bovine serum albumin, pH 7.4), and incubating for 20 min.

Optical setup for spinning disk, total internal reflection fluorescence, and scanning angle interference microscopy

Imaging was performed on one of two Nikon TI-E microscopes equipped with a Nikon 60x Plan Apo VC 1.20 NA water immersion objective, or a Nikon 100x Plan Apo 1.49 NA oil immersion objective, and four laser lines (405, 488, 561, 640 nm), either a Hamamatsu Flash 4.0 or Andor iXon EM-CCD camera, and μManager software [Edelstein, et al., 2010]. A polarizing filter was placed in the excitation laser path to polarize the light perpendicular to the plane of incidence. Angle of illumination was controlled with either a standard Nikon TIRF motorized positioner or a mirror moved by a motorized actuator (Newport, CMA-25CCCL). Scanning angle microscopy was performed and analyzed as previously described [Carbone, et al., 2016].

Reconstitution of membrane interfaces

Proteins were diluted in reaction buffer (50 mM HEPES, 150 mM NaCl, 1 mM TCEP, 1 mg/mL bovine serum albumen, pH 7.4) and then mixed 2:1 with GUVs, or added to supported lipid bilayers. 1 h after mixing, supported lipid bilayers were washed three times with reaction buffer and GUVs were added. Rapamycin (Sigma, R0395) was added to FRB-FKBP reactions at a final concentration of 1 mM. GUVs were allowed to settle for 30-60 min prior to imaging.

Image analysis

Images were analyzed using FIJI software [Schindelin, et al., 2012]. To calculate percent exclusion values, regions of interest (ROIs) were selected from protein of interest enriched and depleted zones of the GUV-SLB interface. The ratio of the mean pixel values for each GUV zone was calculated. This ratio was expressed as a percent corresponding to (1-(depleted/enriched))*100.

ACKNOWLEDGEMENTS

We would like to thank N. Stuurman for help with microscopy and image analysis and M. Taylor for guidance with protein purification and DNA tethering. We thank A. Williamson, N Stuurman, and M. Morrissey for comments on the manuscript. The authors acknowledge funding from the the Howard Hughes Medical Institute and National Institutes of Health (R01EB007187, R.D.V.).

COMPETING INTERESTS

The authors do not declare any competing interests.

REFERENCES

Brownlie, R. J., & Zamoyska, R. (2013). T cell receptor signalling networks: branched, diversified and bounded. *Nature Reviews Immunology*, *13*(4), 257–269. http://doi.org/10.1038/nri3403

Davis, S. J., & van der Merwe, P. A. (2006). The kinetic-segregation model: TCR triggering and beyond. *Nature Immunology*, *7*(8), 803–809. http://doi.org/10.1038/ni1369

Woollett, G. R., Williams, A. F., & Shotton, D. M. (1985). Visualisation by low-angle shadowing of the leucocyte-common antigen. A major cell surface glycoprotein of lymphocytes. *The EMBO Journal*, *4*(11), 2827–30. Retrieved from http://www.ncbi.nlm.nih.gov/pubmed/2933249

McCall, M. N., Shotton, D. M., & Barclay, A. N. (1992). Expression of soluble isoforms of rat CD45. Analysis by electron microscopy and use in epitope mapping of anti-CD45R monoclonal antibodies. *Immunology*, *76*(2), 310–7. Retrieved from http://www.ncbi.nlm.nih.gov/pubmed/1378817

Chang, V. T., Fernandes, R. A., Ganzinger, K. A., Lee, S. F., Siebold, C., McColl, J., … Davis, S. J. (2016). Initiation of T cell signaling by CD45 segregation at “close contacts.” *Nature Immunology*, *17*(5), 574–582. http://doi.org/10.1038/ni.3392

Birnbaum, M. E., Mendoza, J. L., Sethi, D. K., Dong, S., Glanville, J., Dobbins, J., … Garcia, K. C. (2014). Deconstructing the Peptide-MHC Specificity of T Cell Recognition. *Cell*, *157*(5), 1073–1087. http://doi.org/10.1016/j.cell.2014.03.047

Varma, R., Campi, G., Yokosuka, T., Saito, T., & Dustin, M. L. (2006). T Cell Receptor-Proximal Signals Are Sustained in Peripheral Microclusters and Terminated in the Central Supramolecular Activation Cluster. *Immunity*, *25*(1), 117–127. http://doi.org/10.1016/j.immuni.2006.04.010

James, J. R., & Vale, R. D. (2012). Biophysical mechanism of T-cell receptor triggering in a reconstituted system. *Nature*. http://doi.org/10.1038/nature11220

Cordoba, S.-P., Choudhuri, K., Zhang, H., Bridge, M., Basat, A. B., Dustin, M. L., & van der Merwe, P. A. (2013). The large ectodomains of CD45 and CD148 regulate their segregation from and inhibition of ligated T-cell receptor. *Blood*, *121*(21), 4295–4302. http://doi.org/10.1182/blood-2012-07-442251

Banaszynski, L. A., Liu, C. W., & Wandless, T. J. (2005). Characterization of the FKBP·Rapamycin·FRB Ternary Complex. *Journal of the American Chemical Society*, *127*(13), 4715–4721. http://doi.org/10.1021/ja043277y

Taylor, M. J., Husain, K., Gartner, Z. J., Mayor, S., & Vale, R. D. (2016). *Signal Transduction Through a DNA-Based T Cell Receptor*. Retrieved from http://biorxiv.org/lookup/doi/10.1101/062877

Chi, Q., Wang, G., & Jiang, J. (2013). The persistence length and length per base of single-stranded DNA obtained from fluorescence correlation spectroscopy measurements using mean field theory. *Physica A: Statistical Mechanics and Its Applications*, *392*(5), 1072–1079. http://doi.org/10.1016/j.physa.2012.09.022

Gautier, A., Juillerat, A., Heinis, C., Corrêa, I. R., Kindermann, M., Beaufils, F., & Johnsson, K. (2008). An Engineered Protein Tag for Multiprotein Labeling in Living Cells. *Chemistry & Biology*, *15*(2), 128–136. http://doi.org/10.1016/j.chembiol.2008.01.007

Chung, M., Koo, B. J., & Boxer, S. G. (2013). Formation and analysis of topographical domains between lipid membranes tethered by DNA hybrids of different lengths. *Faraday Discuss.*, *161*, 333–345. http://doi.org/10.1039/C2FD20108A

Schmid, E. M., Bakalar, M. H., Choudhuri, K., Weichsel, J., Ann, H. S., Geissler, P. L., … Fletcher, D. A. (2016). Size-dependent protein segregation at membrane interfaces. *Nature Physics*, *12*(7), 704–711. http://doi.org/10.1038/nphys3678

Hermiston, M. L., Xu, Z., & Weiss, A. (2003). CD45: A Critical Regulator of Signaling Thresholds in Immune Cells. *Annual Review of Immunology*, *21*(1), 107–137. http://doi.org/10.1146/annurev.immunol.21.120601.140946

Chui, D., Ong, C. J., Johnson, P., Teh, H. S., & Marth, J. D. (1994). Specific CD45 isoforms differentially regulate T cell receptor signaling. *The EMBO Journal*, *13*(4), 798–807. Retrieved from http://www.ncbi.nlm.nih.gov/pubmed/7509278

Czyzyk, J., Leitenberg, D., Taylor, T., & Bottomly, K. (2000). Combinatorial Effect of T-Cell Receptor Ligation and CD45 Isoform Expression on the Signaling Contribution of the Small GTPases Ras and Rap1. *Molecular and Cellular Biology*, *20*(23), 8740–8747. http://doi.org/10.1128/MCB.20.23.8740-8747.2000

Okumura, M., Matthews, R. J., Robb, B., Litman, G. W., Bork, P., & Thomas, M. L. (1996). Comparison of CD45 extracellular domain sequences from divergent vertebrate species suggests the conservation of three fibronectin type III domains. *Journal of Immunology*, *157*(4), 1569–75. Retrieved from http://www.ncbi.nlm.nih.gov/pubmed/8759740

Gascoigne, N. R. J., Zal, T., & Alam, S. M. (2001). T-cell receptor binding kinetics in T-cell development and activation. *Expert Reviews in Molecular Medicine*, *3*(6). http://doi.org/10.1017/S1462399401002502

Carbone, C. B., Vale, R. D., & Stuurman, N. (2016). An acquisition and analysis pipeline for scanning angle interference microscopy. *Nature Methods*, *13*(11), 897–898. http://doi.org/10.1038/nmeth.4030

Liang, J., Choi, J., & Clardy, J. (1999). Refined structure of the FKBP12-rapamycin-FRB ternary complex at 2.2 A resolution. *Acta Crystallographica. Section D, Biological Crystallography*, *55*(Pt 4), 736–44. Retrieved from http://www.ncbi.nlm.nih.gov/pubmed/10089303

Chen, L., & Flies, D. B. (2013). Molecular mechanisms of T cell co-stimulation and co-inhibition. *Nature Reviews Immunology*, *13*(4), 227–242. http://doi.org/10.1038/nri3405

Lin, D. Y. -w., Tanaka, Y., Iwasaki, M., Gittis, A. G., Su, H.-P., Mikami, B., … Garboczi, D. N. (2008). The PD-1/PD-L1 complex resembles the antigen-binding Fv domains of antibodies and T cell receptors. *Proceedings of the National Academy of Sciences*, *105*(8), 3011–3016. http://doi.org/10.1073/pnas.0712278105

Butte, M. J., Peña-Cruz, V., Kim, M.-J., Freeman, G. J., & Sharpe, A. H. (2008). Interaction of human PD-L1 and B7-1. *Molecular Immunology*, *45*(13), 3567–3572. http://doi.org/10.1016/j.molimm.2008.05.014

Hui, E., Cheung, J., Zhu, J., Su, X., Taylor, M. J., Wallweber, H. A., … Vale, R. D. (2016). *T cell co-stimulatory receptor CD28 is a primary target for PD-1-mediated inhibition*. Retrieved from http://biorxiv.org/lookup/doi/10.1101/086652

Carrie Miceli, M., Moran, M., Chung, C. D., Patel, V. P., Low, T., & Zinnanti, W. (2001). Co-stimulation and counter-stimulation: lipid raft clustering controls TCR signaling and functional outcomes. *Seminars in Immunology*, *13*(2), 115–128. http://doi.org/10.1006/smim.2000.0303

Su, X., Ditlev, J. A., Hui, E., Xing, W., Banjade, S., Okrut, J., … Vale, R. D. (2016). Phase separation of signaling molecules promotes T cell receptor signal transduction. *Science*, *352*(6285), 595–599. http://doi.org/10.1126/science.aad9964

Wilson, D. B., Pinilla, C., Wilson, D. H., Schroder, K., Boggiano, C., Judkowski, V., … Houghten, R. A. (1999). Immunogenicity. I. Use of peptide libraries to identify epitopes that activate clonotypic CD4+ T cells and induce T cell responses to native peptide ligands. *Journal of*

Immunology (Baltimore, Md. : 1950), *163*(12), 6424–34. Retrieved from http://www.ncbi.nlm.nih.gov/pubmed/10586032

Farlow, J., Seo, D., Broaders, K. E., Taylor, M. J., Gartner, Z. J., & Jun, Y. (2013). Formation of targeted monovalent quantum dots by steric exclusion. *Nature Methods*, *10*(12), 1203–1205. http://doi.org/10.1038/nmeth.2682

Schmid, E. M., Richmond, D. L., & Fletcher, D. A. (2015). Reconstitution of proteins on electroformed giant unilamellar vesicles (pp. 319–338). http://doi.org/10.1016/bs.mcb.2015.02.004

Edelstein, A. D., Tsuchida, M. A., Amodaj, N., Pinkard, H., Vale, R. D., & Stuurman, N. (2014). Advanced methods of microscope control using μManager software. *Journal of Biological Methods*, *1*(2), 10. http://doi.org/10.14440/jbm.2014.36

Schindelin, J., Arganda-Carreras, I., Frise, E., Kaynig, V., Longair, M., Pietzsch, T., … Cardona, A. (2012). Fiji: an open-source platform for biological-image analysis. *Nature Methods*, *9*(7), 676–682. http://doi.org/10.1038/nmeth.2019

MAIN FIGURES

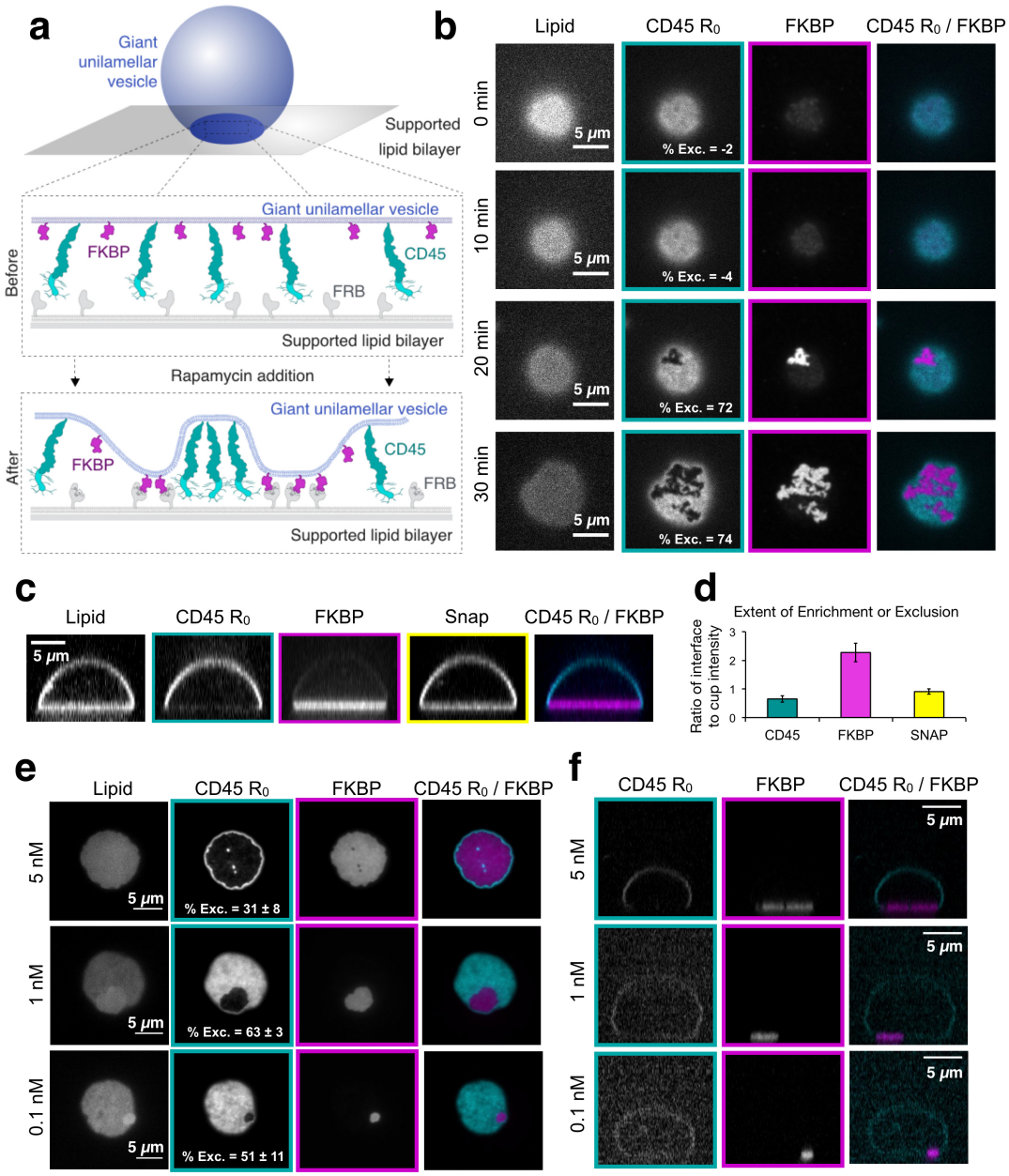

Figure 1.

Receptor-ligand binding induces CD45 segregation at membrane interfaces.

(**a**) Schematic of rapamycin induced receptor (FKBP)-ligand (FRB) binding and CD45 R_0 segregation between a giant unilamellar vesicle (GUV) and a supported lipid bilayer (SLB) (**b**) Total internal reflection fluorescence (TIRF) microscopy of a GUV-SLB interface at indicated times after rapamycin addition, showing concentration of FKBP into microdomains that exclude CD45 R_0. Percent exclusion of CD45 R_0 is indicated for each image shown. (**c**) Spinning disk z-sections of GUVs after membrane-apposed interfaces have reached equilibrium, showing localization of FKBP to the membrane interface, localization of CD45 R_0 away from the interface, and uniform distribution of SNAP. (**d**) Quantification of experiment shown in **c**; mean ± standard deviation (n=7 GUVs from one representative experiment). (**e**) Titration of FKBP concentration (indicated at left of images) with constant CD45 R_0 concentration imaged by TIRF microscopy. Percent exclusion of CD45 R_0 indicated as mean ± standard deviation with n=5 GUVs per condition from one representative experiment. (**f**) Spinning disk z-sections of GUVs shown in **e**.

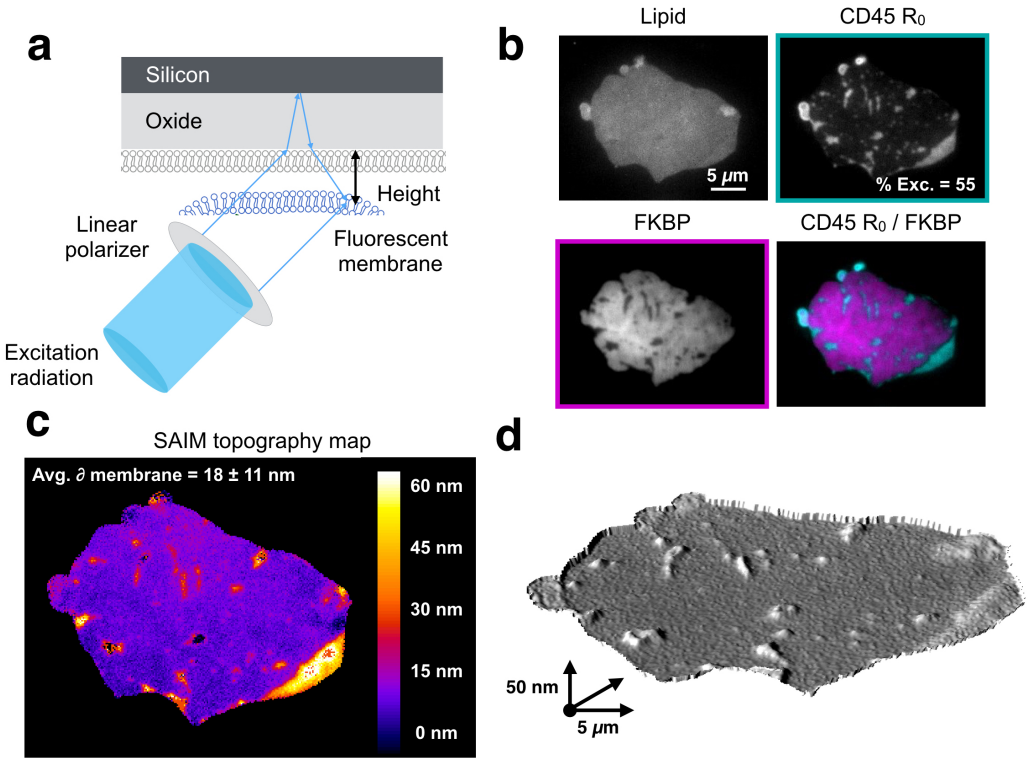

Figure 2.

Membrane topology is influenced by local protein composition.

(**a**) Schematic of scanning angle interference microscopy showing reflection and interference of excitation light that produces structured illumination patterns used to deduce fluorophore height, adapted from Carbone, et al., 2016. (**b**) Epifluorescence microscopy showing localization of lipid, CD45 R_0 and FKBP on GUV analyzed by SAIM imaging. Percent exclusion of CD45 R_0 indicated for image shown. (**c**) SAIM reconstruction of GUV membrane derived from lipid fluorescence showing an increase in membrane height at CD45 R_0 clusters. Average membrane height change depicted as mean ± standard deviation, n=4-6 clusters from each of 4 GUVs imaged during two separate experiments. (**d**) 3D model of data shown in **c**. Z-scale is exaggerated to clearly depict membrane deformations.

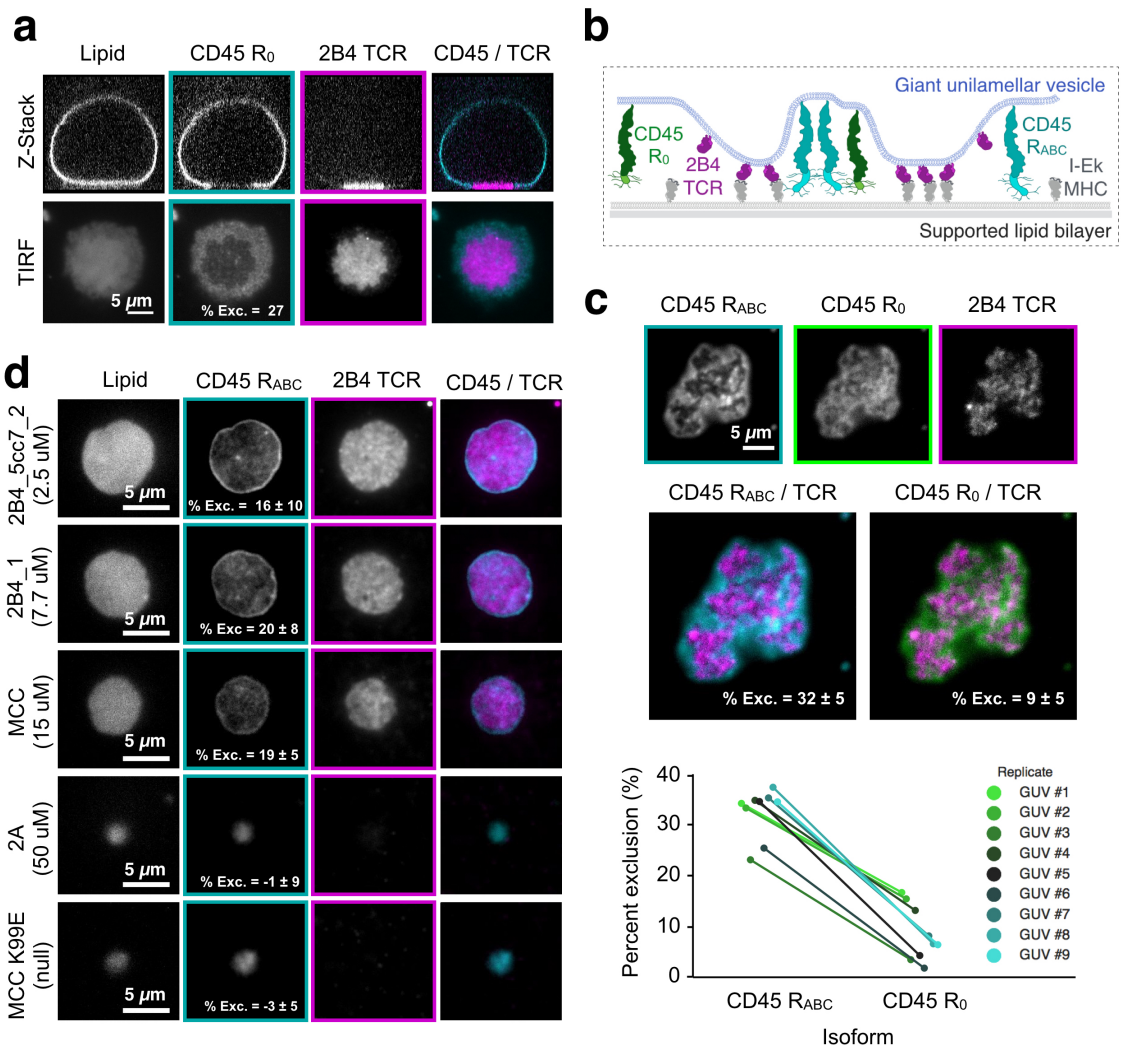

Figure 3.

TCR-pMHC binding induces CD45 segregation at membrane interfaces.

(**a**) Top, spinning disk z-sections of GUVs after membrane-apposed interfaces have reached equilibrium, showing localization of 2B4 TCR to membrane interface and exclusion CD45 R_0 away from the interface. Bottom, TIRF images of GUV-SLB interface for GUV shown in panel above. Percent exclusion of CD45 R_0 indicated for image shown. (**b**) Schematic of 2B4 TCR-IE^k MHC binding between a GUV and a SLB, and segregating away from two CD45 isoforms (R_0 and R_{ABC}). (**c**) Top, segregation of CD45 R_0 and CD45 R_{ABC} on the same GUV membrane away from 2B4 TCR, shown by TIRF microscopy of membrane interface. Percent exclusion of CD45 isoforms indicated as mean ± standard deviation, with n=9 GUVs from one representative experiment. Bottom, graphical representation of data shown in top panel. (**d**) Dependence of CD45 R_{ABC} exclusion as a function of TCR-pMHC affinity using peptides with different K_Ds, indicated at left of images. Imaged by TIRF microscopy of membrane interfaces. Percent exclusion of CD45 R_{ABC} indicated as mean ± standard deviation, n=5,5,2,4,5 GUVs from one representative experiment.

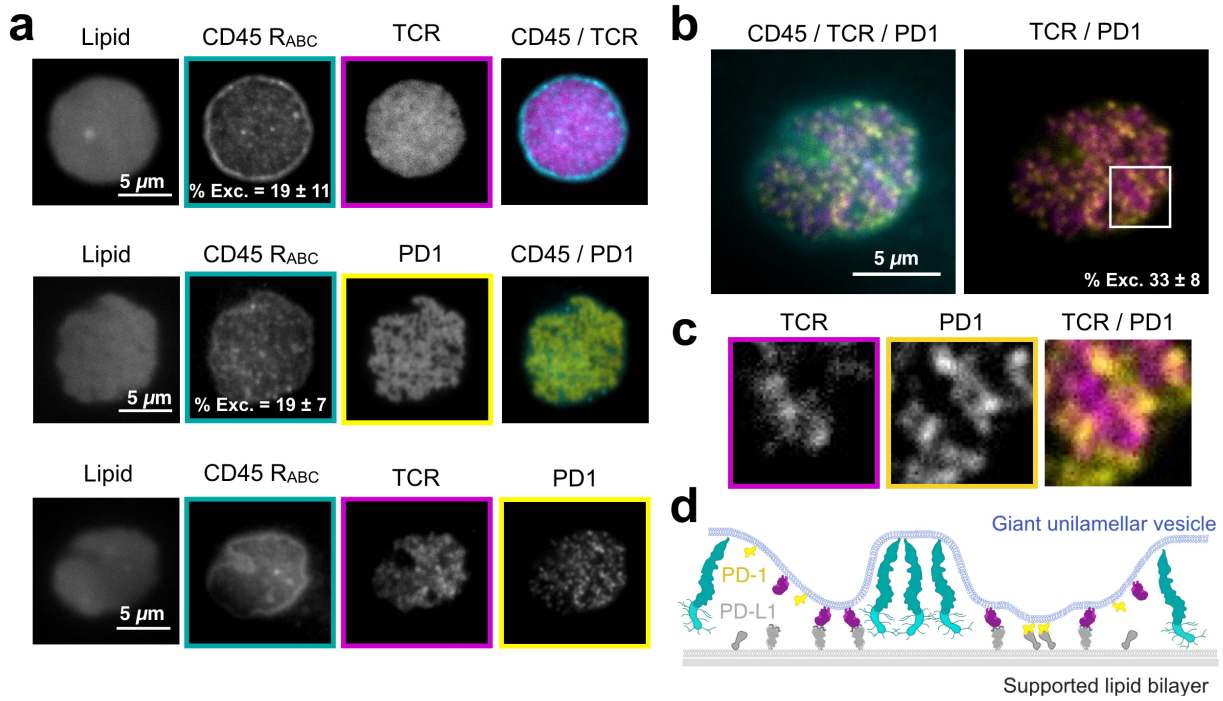

Figure 4.

The inhibitory co-receptor PD-1 partitions away from CD45 and TCR.

(**a**) Top, TIRF microscopy of a GUV-SLB interface at equilibrium showing concentration of TCR into microdomains that exclude CD45 R_{ABC}. Percent exclusion of CD45 R_{ABC} indicated as mean ± standard deviation, n=11 GUVs from one representative experiment. Middle, TIRF microscopy showing concentration of PD-1 into microdomains that exclude CD45 R_{ABC}. Percent exclusion of CD45 R_{ABC} indicated as mean ± standard deviation, n=9 GUVs from one representative experiment. Bottom, TIRF microscopy showing concentration of TCR and PD-1 into separate microdomains that exclude CD45 R_{ABC}. (**b**) Merged channels from **a**, bottom, to highlight protein segregation. Percent exclusion of PD-1 from TCR indicated as mean ± standard deviation, n=5 GUVs from one representative experiment. (**c**) Enlarged image of inset in **b** showing TCR and PD-1 segregation. (**d**) Schematic of 2B4 TCR-IE^k MHC and PD-1-PD-L1 binding between a GUV and a SLB, with segregation away from CD45 R_{ABC}.